Habit planes of climbing and gliding dislocations in TiAl determined in three dimensions by electron tomography

Jean-Philippe Monchoux, Daniel Ferry

Habit planes of climbing and gliding dislocations in TiAl determined in three dimensions by electron tomography

Jean-Philippe Monchoux[1]*, Daniel Ferry[2]

[1]CEMES, CNRS, Université de Toulouse; Toulouse, 31055, France. E-mail : monchoux@cemes.fr

[2]Aix Marseille Univ, CNRS, CINaM; Marseille, 13009, France. E-mail : daniel.ferry@cnrs.fr

*Corresponding author. Email: monchoux@cemes.fr

Abstract:

In this study, the habit planes of dislocations moving by glide and climb at 850°C-900°C have been determined in three dimensions (3D) by electron tomography, using the TiAl intermetallics as a model system. An almost complete digital 3D reconstruction approach has been implemented, based on algorithms developed in life sciences, with which the habit planes orientations have been obtained with ± 5° accuracy. It could thus be demonstrated, notably, that climbing $a[001]$ pure edge dislocations loops, previously identified in literature, actually constitute Bardeen-Herring sources. Moreover, mixed-climb in {011) planes has been properly evidenced, as well as coexistence of gliding and climbing dislocation segments in the same region of the crystal. Consequently, improving the material's strength at 850-900°C would require controlling both the glide and climb mechanisms by means of suitable solutes.

Keywords: Dislocations; Electron tomography; 3D reconstruction

Main text

To widen the industrial use of TiAl-based alloys, the operation temperatures have to reach 800°C and above [1]. However, the microscopic mechanisms controlling the mechanical deformation of the TiAl alloys at these temperatures are not yet fully described and interpreted, which is necessary to propose design guidelines aiming at improving the strength of these materials. For example, it has been proposed that the kinetics of glide-controlled deformation processes in TiAl alloys can be reduced by addition of C and Si [2, 3], whereas in the case of climb-controlled mechanisms, heavy elements as Nb [4] or W [5, 6] have proved their efficiency. In this context, it is then of primary importance to properly identify the activated deformation mechanisms, and preferably, the controlling one.

For this purpose, it is necessary to obtain a key information, which is the orientation of the Burgers vector $\vec{b}$ of the dislocations with respect to their habit plane *P* (plane in which the

motion of the dislocation takes place). Thus, $\vec{b}$ contained in P shows glide, whereas $\vec{b}$ making any angle with P indicates glide and climb (glide of jogged dislocations [7]), often simply referred to as climb [8], since the climb contribution usually controls the kinetics of dislocation motion. Finally, $\vec{b}$ perpendicular to P corresponds to pure climb, and results from the creation of Bardeen-Herring dislocation loops [9]. Therefore, identifying the mechanisms relies on the determination of the orientation of the Burgers vector (obtained by the invisibility $\vec{g} \cdot \vec{b} = 0$ criterion), and of the habit planes, for which geometrical determination procedures of the orientation of dislocation loops using inclination of the sample holder have been developed [6]. However, an intrinsic limitation of these methods is that the two extremities of the loops have to emerge from the same side of the thin foils, which is only the case in a proportion of about one over two of the investigated loops. Moreover, to obtain data accurate enough (orientations determined within $\pm 5°$), the projected width of loops have to be determined for a set of diffraction conditions, corresponding typically to 5-10 inclinations of the sample holder, by use of manual procedures which can be tedious. Another possibility is to determine the habit plane orientation by inclining the sample holder in such a way that the loop is positioned edge-on with respect to the observation plane [10]. However, this method is also limited to few favorable situations.

Nevertheless, using these approaches, the deformation mechanisms in TiAl alloys at high temperatures were identified during the past decades. Most of the studies show that between 550°C and 900°C, climb and glide coexist [6, 11-14]. Recently, *in-situ* TEM observations have shown that dislocations moving by climb and glide can exhibit similar velocities, an observation which gives an interpretation to the coexistence of these two mechanisms [10]. From 850°C and above, other mechanisms are reported: glide of ordinary dislocations in non-compact planes [15], increased activation of superdislocations [16], or formation of c-type $a[001]$ dislocations [17]. From the above literature analysis, it can be seen that, despite the strong technological interest of the TiAl alloys, proper identification of the microscopic deformation mechanisms required two decades, probably because of the complexity of the TEM investigations.

In this paper, we aim to show that microscopic deformation mechanisms in the model TiAl system can be easily elucidated using emerging 3D reconstruction approaches. The very recent developments in the determination of the 3D morphology of dislocations by electron tomography have shown that a breakthrough in this field is now possible, inducing tremendous interest [18-25]. Tomography, in the general case, consists in reconstructing the 3D morphology of an object from a tilted series of its 2D projections [24, 26]. In the particular case of studying dislocation structures, the specific conditions under which dislocations are visible need to be maintained for all the images in the tilted series. This is achieved by positioning the specimen in the sample holder in such a way that a diffraction vector $\vec{g}$, for which the dislocations are visible, is parallel to the tilt axis. A tilted series is then acquired typically with steps of 1-2°. For a high accuracy 3D reconstruction, each image in the tilted series has to be very accurately aligned on a common tilt axis by implementing shift and rotation corrections of drift occurring during acquisition (image registration). Most commonly, cross-correlation techniques or least-square tracking

methods of fiducial markers (*e.g.*, gold beads) are used [26, 27]. Alternative methods using stereographic triangulation [28] and dislocation detection by deep neural network [25] have been developed to enable 3D reconstructions from image pairs. The methods for 3D reconstruction of dislocation structures were first introduced by Barnard et al. [18]. They were employed to reveal dislocation structures at crack tips [19], around precipitates [20] and in sub-boundaries [24]. Finally, a review on these approaches was proposed [24]. However, a major contribution comes from Mussi et al's team, who has devoted several studies to the development of electron tomography for investigating various dislocation mechanisms in olivine [21], zirconium [23] and MgO [22]. Notably, habit planes for glide and climb mechanisms were determined [22].

In this work, we identified image alignment as the key parameter to result in high quality tomograms. Little information is given in literature concerning this important step, reference being made to manual procedures [21-23], or no procedure being indicated [18, 19], the only more precise work on this point being that of Liu et al. [20], who reports the use of nanometer-size defects or dislocation junction, acting as fiducial markers for alignment. Here, we employed a robust image registration procedure based on the production of landmark chains throughout the tilted series [27]. This technique was first applied in life sciences but has also been successfully extended to study the structure and topology of nano- & mesopore networks in organic matter present in shale rocks [29, 30]. It is described in details in the Materials and method section of the Supplementary materials. The main advantage of this method is that an accurate alignment of curvilinear structures such as dislocations can be achieved without the use of fiducial markers deposited onto the sample, or already present (defects, junctions [20]) prior to recording the tilted series. Moreover, this is an almost complete digital procedure, in which manual adjustments are minimized. As a result, high-quality alignment of the tilted series is obtained, giving tomograms with high spatial resolution even for complex dislocation sub-structures. Supplementary Figure 1 shows that the 3D reconstructions reproduce the images obtained by TEM without noticeable distortion, that the lateral accuracy of the reconstructions (≈ 12 nm) can be as low as 2-3 times that of our microscope (≈ 5 nm), and that the habit planes orientations can be determined within ± 5°.We employed this method in the case of the ordered intermetallic $L1_0$ γ-TiAl phase, because the atomic ordering of Ti and Al results most of the time of only two dislocation families of Burgers vectors $\vec{b} = a/2\,[110]$ and $\vec{b} = a/2\,[1\bar{1}0]$ (with a: lattice constant) [31]. Under given diffraction conditions, like $\vec{g} = \langle 111 \rangle$, only one dislocation family is in contrast and the mechanisms can thus be selectively determined (note also that, due to chemical order, $\langle uvw]$ and $\{hkl)$ conventions for permutation of the indices can be used [32]). Hence, using this model system, typical glide and climb dislocation processes can be easily investigated. At high temperatures, however, dislocations of Burgers vector $\vec{b} = a[001]$ also contribute to the deformation [17]. TiAl alloys were then deformed at 850°C to 900°C by low (1.5-2 %) and high (20 %) amounts, at 10^{-4} s^{-1} and 6×10^{-8} s^{-1} deformation rates. Details on sample preparation are given in the Materials and methods section of the Supplementary materials.

We show hereafter the relevance of using this 3D reconstruction approach to elucidate the dislocation mechanisms in TiAl through precise determination of the habit planes, as was also

carried out in MgO using electron tomography [22]. In some cases, tomograms were analyzed for tilt values higher than $\approx \pm 60°$, which are not accessible through the microscope. The tomograms of our study are given as Supplementary materials, with corresponding Movies to visualize them. Thus, Supplementary Movie 1 evidences that some segments move by gliding while others move by climbing in the dislocation family of Burgers vector $\vec{b} = a/2\,[110]$ (Fig. 1a schematically depicts these two mechanisms). Fig. 1b-d illustrate that these mechanisms can be readily deduced from the 3D reconstructions.

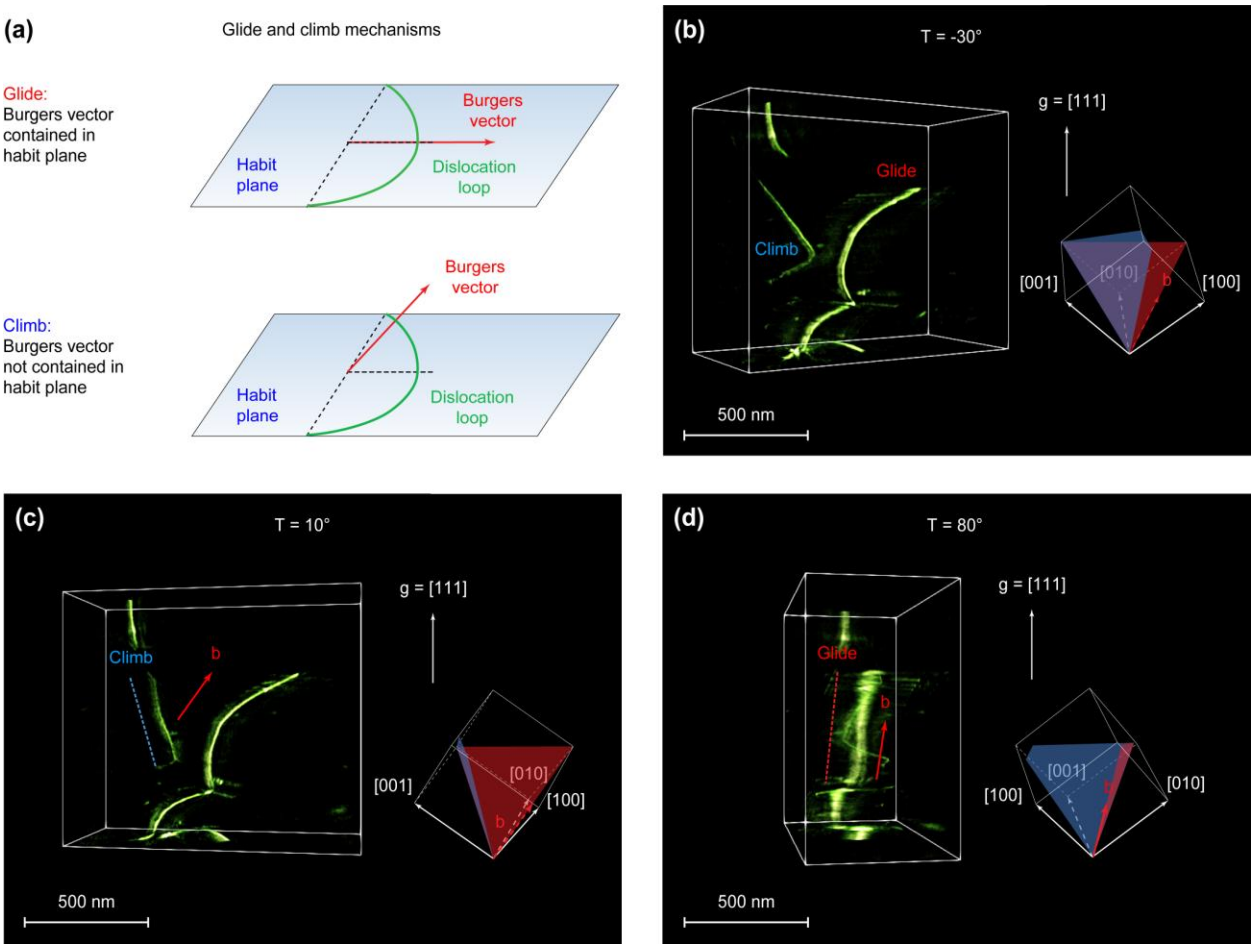

Fig. 1. Examples of glide and climb mechanisms (GE TiAl alloy deformed by 2 % at 10^{-4} s^{-1} deformation rate in compression at 900°C). (a) Schematic drawings showing the orientation of the habit plane of portions of dislocation loops for glide and climb mechanisms. (b) 3D reconstruction at tilt T = -30° of a region where gliding and climbing dislocation segments coexist, in the orthonormal coordinate system of the crystal(determined by diffraction analyses, not shown, giving the orientation of the diffracting planes with respect to the tilt axis, with typically ± 2° accuracy). For these dislocations, the Burgers vector $\vec{b}$ is equal to $a/2\,[110]$. (c) Habit plane of the first loop edge-on that does not contain the Burgers vector, demonstrating a climb mechanism (tilt T = 10°). (d) Habit plane of the second loop edge-on that is parallel to the Burgers vector, evidencing a glide mechanism (tilt T = 80°). See also Supplementary Movie 1.

Supplementary Movie 2 shows planar dislocation loops, in a region which was investigated in the study of Naanani *et al.* [17]. In the present work, a tilted series is recorded under residual contrast conditions ($\vec{g}\cdot\vec{b}=0$ and $\vec{g}\cdot(\vec{b}\wedge\vec{u})\neq 0$, with $\vec{g}=[110]$, $\vec{b}=a[001]$ and $\vec{u}$: dislocation line vector contained in the habit plane), which allows 3D reconstruction despite a low signal-to-noise ratio. In the study of Naanani *et al.*, it was shown that the dislocation labelled *S* in Fig. 2a was constituted of edge segments of $a[001]$ Burgers vector moving by pure climb in the (001) plane. In the present work, 3D analyses establish that the $a[001]$ segments labelled 1, 2 and 3 also move in the (001) plane (Figs. 2b-c). We therefore show that the dislocation labelled *S* is in fact a source, from which the segments 1, 2 and 3 are generated by the Bardeen-Herring mechanism [9]. Consequently, a correct identification and description of a Bardeen-Herring mechanism is only possible here through 3D reconstruction. In the case of $a/2\langle 110]$ dislocations, growth of Bardeen-Herring loops was observed during *in-situ* TEM observations [13], but no information regarding the habit planes was mentioned. In our study, the habit plane is accurately determined, allowing us to unambiguously identify the mechanism, which is here pure climb of $a[001]$ edge dislocations.

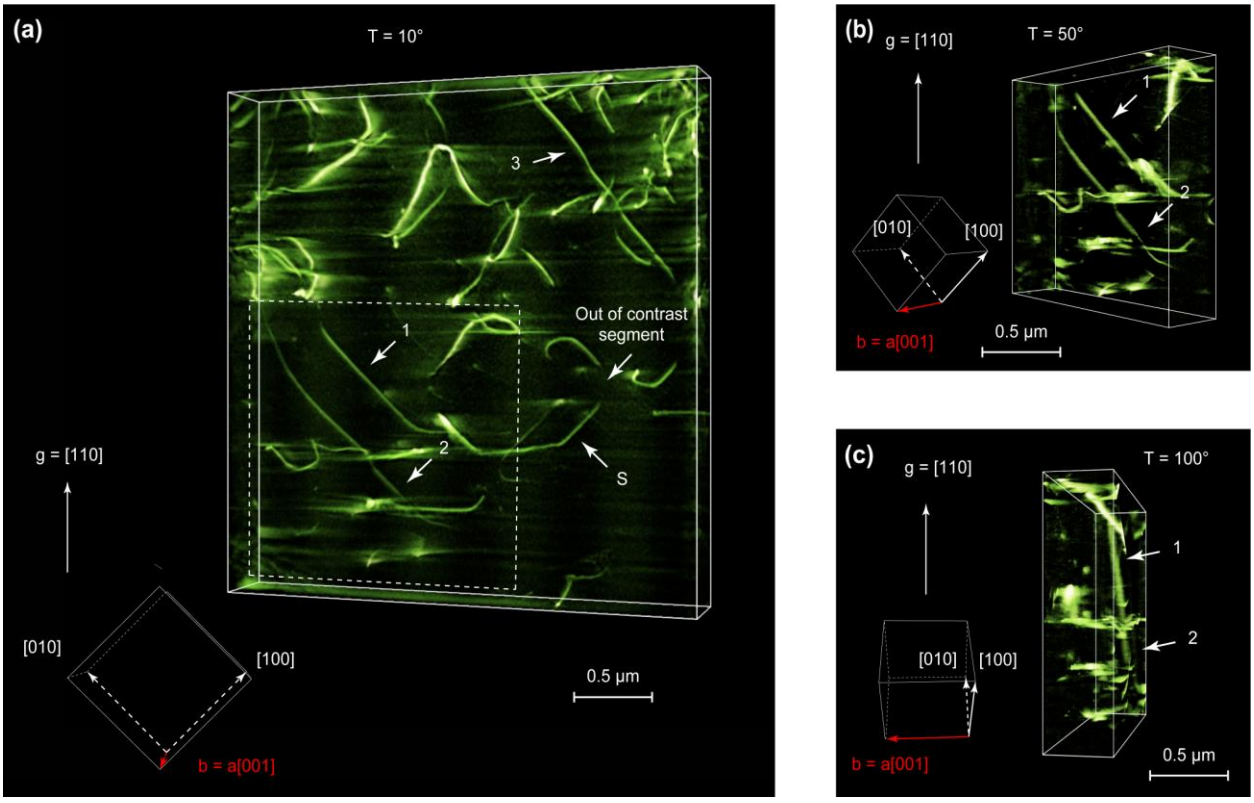

Fig. 2. 3D reconstruction from TEM images recorded in residual contrast conditions ($\vec{g}\cdot(\vec{b}\wedge\vec{u})\neq 0$) of a Bardeen-Herring source (IRIS TiAl alloy deformed by 1.5 % at 6×10^{-8} s^{-1} deformation rate at 850°C). Three loops, labelled 1 to 3, truncated by the TEM thin foil surfaces, have grown from a source, labelled as S. (a) General view at tilt T = 10°. Note that one segment

of the source S is out of contrast, due to fulfilment of the extinction criterion in the residual contrast conditions (the dislocation line vector $\vec{u}$ is in this case parallel to the diffraction vector $\vec{g}$, leading to $\vec{g} \cdot (\vec{b} \wedge \vec{u}) = 0$). (b-c) Details of the region delineated in view (a) at tilts T = 50° and T = 100°, showing notably in view (c) that the habit plane of the planar loops 1 and 2 is perpendicular to the Burgers vector $\vec{b}$, thus highlighting pure climb of $a[001]$ dislocations by a Bardeen-Herring mechanism. See also Supplementary Movie 2.

Finally, Supplementary Movies 3, 4 and 5 show dislocation reorganization in sub-boundaries of complex 3D structure after high plastic deformation (ε = 20 %) at 900°C. It is usually very difficult to perform TEM studies of samples deformed to such elevated level, due to the very high dislocation density, which induces very complex sub-structures. Notwithstanding, the accuracy of the 3D reconstruction, illustrated in Supplementary Movie 3 and Fig. 3a, allows resolving highly interwoven dislocation structures. Analysis of the reconstructed volume shown in Supplementary Movie 4 indicates that the habit planes of the long loops labeled 1, 2 and 3 in Fig. 3b are of $(01\bar{1})$ type, demonstrating climb in compact planes. A detailed 3D reconstruction shown in Supplementary Movie 5 reveals that the sub-boundary plane is close to (101), as reported in Fig. 3c. Therefore, we deduce that the formation of the sub-boundary results from the motion of dislocations in the $(01\bar{1})$ planes as well as from their rearrangement in the (101) planes, as schematically represented in Fig. 4d, both of which involve climb. Because the emergence points of the loops 1, 2 and 3 are not located on the same faces of the TEM thin foil (cf. Supplementary Movie 4), it would have been impossible to determine the habit plane by measuring the projected width of the loops, as described above. Moreover, Fig. 3b shows that orienting the habit plane of the loops edge-on requires tilting the volume by 67°, which is experimentally not possible with conventional sample holders. Therefore, the only way here to determine the habit plane and hence, the mechanism, is to use a 3D approach. Thus, climb in $\{011)$ close-packed planes, which has been occasionally observed in our previous study [6], is here clearly established.

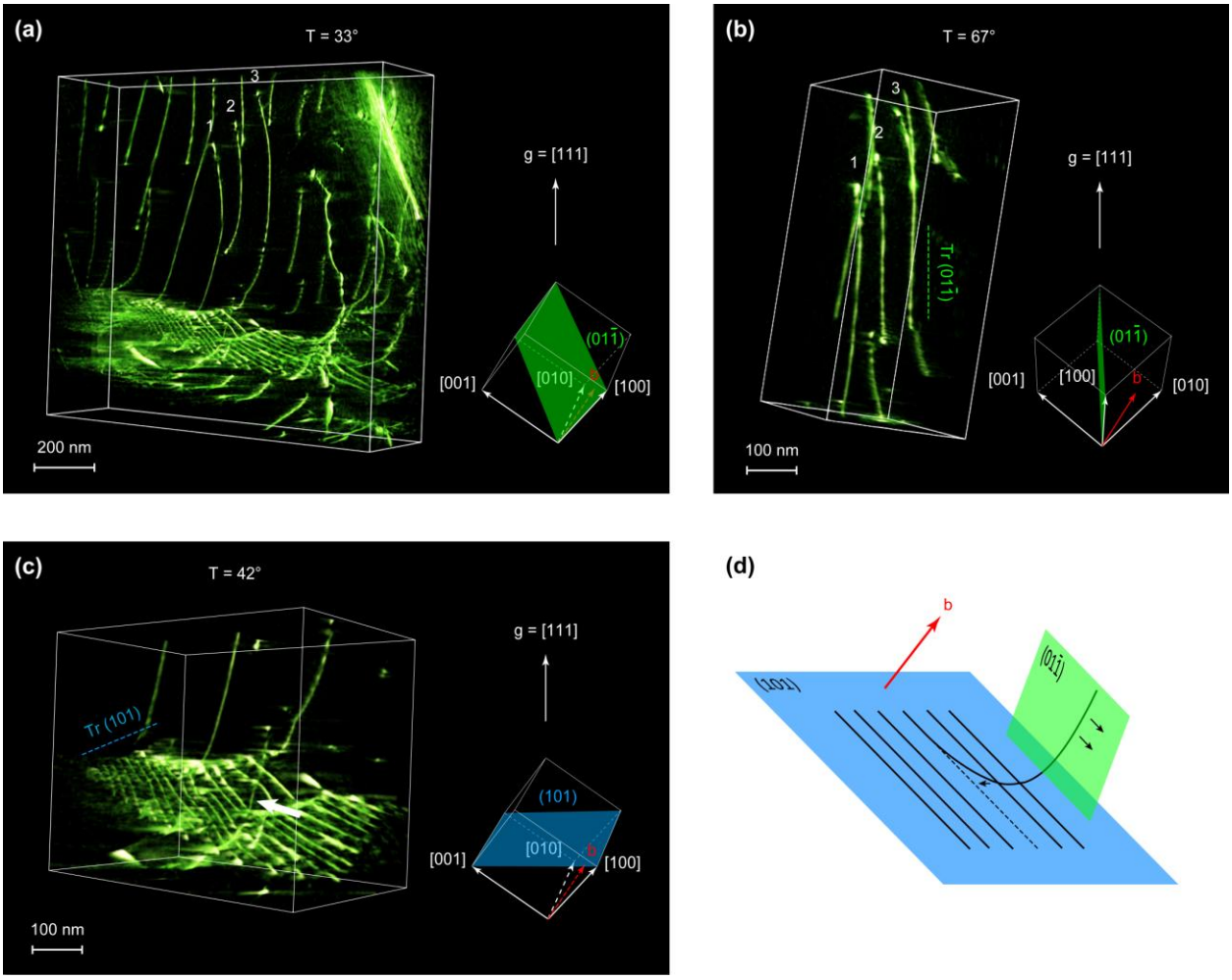

Fig. 3. 3D morphology of a complex dislocation sub-structure (GE TiAl alloy deformed by 20 % at 10^{-4} s^{-1} deformation rate in compression at 900°C). (a) General view at tilt T = 33° showing the orientation of the investigated volume in orthonormal coordinates. See also Supplementary Movie 3. (b) Detailed image at tilt T = 67° showing the dislocations labelled 1, 2 and 3 in view (a) in edge-on position, identifying a compact $(01\bar{1})$ *habit plane resulting from climb. See also Supplementary Movie 4. (c) Detailed image tilt T = 42° showing the dislocation (marked by an arrow) re-arranging in a sub-boundary dislocation network parallel to the compact* (101) *plane by climb. See also Supplementary Movie 5. (d) Schematic drawing illustrating the formation of the sub-boundary network by climb in the* $(01\bar{1})$ *and* (101) *compact planes.*

In summary, the habit planes of dislocations in TiAl have been determined accurately (within ± 5°) using an almost complete digital 3D reconstruction approach, allowing easy identification of the mechanisms. Electron tomography is therefore very useful to identify the controlling mechanisms of deformation in TiAl, as was also reported in MgO [22]. For deformed alloys at 850-900°C, this 3D approach has clearly and unambiguously established the formation of $a[001]$ dislocation loops by pure climb from Bardeen-Herring sources. In addition, a process of sub-grain formation, involving climbing in {011) close-packed planes, has been demonstrated.

However, pure glide is also observed. This suggests that the gliding and climbing processes occur at similar kinetics, meaning that both mechanisms must be controlled, using appropriate solutes if the material's strength is to be improved in the 850-900°C temperature range.

Acknowledgments:

This work was funded by a cooperative Austrian-French HITIAL project co-supported by the French Agence Nationale de la Recherche (ANR) and the Austrian Fonds zur Förderung der wissenschaftlichen Forschung (FWF), grant 18-CE91-0008-01.

Supplementary materials

- Materials and methods.
- Supplementary Figure 1: Data giving quantification of the accuracy of the 3D reconstructions.
- Supplementary Tomogram 1 and Supplementary Movie 1: Climbing and gliding dislocations in TiAl deformed at 900°C.
- Supplementary Tomogram 2 and Supplementary Movie 2: Bardeen-Herring loops developed in TiAl at 850°C.
- Supplementary Tomogram 3 and Supplementary Movie 3: Dislocations forming a sub-boundary network in TiAl deformed by 20 % at 900°C. General view.
- Supplementary Tomogram 4 and Supplementary Movie 4: Dislocations forming a sub-boundary network in TiAl deformed by 20 % at 900°C. Detail 1.
- Supplementary Tomogram 5 and Supplementary Movie 5: Dislocations forming a sub-boundary network in TiAl deformed by 20 % at 900°C. Detail 2.

References

[1] B.P. Bewlay, S. Nag, A. Suzuki, M.J. Weimer, TiAl alloys in commercial aircraft engines, Mater. High Temp. 33 (2016) 549–559.

[2] F. Appel, U. Lorenz, M. Oehring, U. Sparka, R. Wagner, Thermally activated deformation mechanisms in micro-alloyed two-phase titanium amminide alloys, Materials Science and Engineering: A 233 (1997) 1-14.

[3] S. W. Kim, P. Wang, M. H. Oh, D. M. Wee, K. S. Kumar, Mechanical properties of Si- and C-doped directionally solidified TiAl–Nb alloys, Intermetallics 12 (2004) 499-509.

[4] F. Appel, J. D. H. Paul, M. Oehring, U. Fröbel, U. Lorenz, Creep behavior of TiAl alloys with enhanced high-temperature capability, Metallurgical and Materials Transactions A 34 (2003) 2149-2164.

[5] T. Voisin, J. P. Monchoux, M. Thomas, C. Deshayes, A. Couret, Mechanical properties of the TiAl IRIS alloy, Metallurgical and Materials Transactions A 47 (2016) 6097-6018.

[6] A. Couret, J. P. Monchoux, D. Caillard, On the high creep strength of the W containing IRIS-TiAl alloy at 850°C, Acta Materialia 181 (2019) 331-341.

[7] J. P. Hirth, J. Lothe, Therory of dislocations (Krieger Publishing Company, 1982).

[8] D. Caillard, J. L. Martin, Thermally activated mechanisms in crystal plasticity (Elsevier, 2003).

[9] K. H. Westmacott, R. S. Barnes, R. E. Smallman, The observation of a dislocation 'Climb' source, Philosophical Magazine 7 (1962) 1585-1596.

[10] B. Galy, M. Musi, M. Hantcherli, G. Molénat, A. Couret, P. Spoerk-Erdely, H. Clemens, J.P. Monchoux, Glide and mixed climb dislocation velocity in γ-TiAl investigated by in-situ transmission electron microscopy, Scripta Materialia 228 (2023) 115333.

[11] B.M. Kad, H.L. Fraser, On the contribution of climb to high-temperature deformation in single phase gamma –TiAl, Philos. Mag. A 69 (1994) 689–699.

[12] B. Viguier, K.J. Hemker, J. Bonneville, F. Louchet, J.L. Martin, Modeling the flow stress anomaly in gamma TiAl. 1. Experimental observations of dislocation mechanisms, Philos. Mag. A 71 (1995) 1295–1312.

[13] F. Appel, R. Wagner, Microstructure and deformation of two-phase γ-titanium aluminides, Mater. Sci. Eng.: R: Rep. 22 (1998) 187–268.

[14] J. Malaplate, D. Caillard, A. Couret, Interpretation of the stress dependence of creep by a mixed climb mechanism in γ-TiAl, Philos. Mag. A 84 (2004) 3671–3687.

[15] H. Inui, M. Matsumuro, D.H. Hu, M. Yamaguchi, Temperature dependence of yield stress, deformation mode and deformation structure in single crystals of TiAl (Ti-56 at% Al), Philos. Mag. A 75 (1997) 395–423.

[16] S.H. Whang, Y.D. Hahn, Positive temperature dependence of the yield stress in $L1_0$-type Ti-Al-V compound, Scr. Metall. Mater. 24 (1990) 4 85–4 90.

[17] S. Naanani, J.P. Monchoux, C. Mabru, A. Couret, Pure climb of [001] dislocations in TiAl at 850 °C, Scripta Materialia 149 (2018) 53-57.

[18] J. S. Barnard, J. Sharp, J. R. Tong, P. A. Midgley, High-resolution three-dimensional imaging of dislocations, Science 313 (2006) 319.

[19] M. Tanaka, K. Higashida, K. Kaneko, S. Hata, M. Mitsuhara, Crack tip dislocations revealed by electron tomography in silicon single crystal, Scripta Materialia 59 (2008) 901-904.

[20] G.S. Liu, I.M. Robertson, Three-dimensional visualization of dislocation-precipitate interactions in a Al–4Mg–0.3Sc alloy using weak-beam dark-field electron tomography, J. Mater. Res 26 (2011) 515-522.

[21] A. Mussi, P. Cordier, S. Demouchy, C. Vanmansart, Characterization of the glide planes of the [001] screw dislocations in olivine using electron tomography, Phys Chem Minerals 41 (2014) 537–545.

[22] A. Mussi, P. Carrez, K. Gouriet, B. Hue, P. Cordier, 4D electron tomography of dislocations undergoing electron irradiation, Comptes Rendus Physique 22 (2021) 67-81.

[23] A. Mussi, A. Addad, F. Onimus, Dislocation electron tomography: A technique to characterize the dislocation microstructure evolution in zirconium alloys under irradiation, Acta Materialia 213 (2021) 116964.

[24] Z. Feng, R. Fu, C. Lin, G. Wu, T. Huang, L. Zhang, X. Huang, TEM-based dislocation tomography: challenges and opportunities, Current Opinion in Solid State and Materials Science 24 (2020) 100833.

[25] O. Altingövde, A. Mishchuk, G. Ganeeva, E. Oveisi, C. Hebert, P. Fua, 3D reconstruction of curvilinear structures with stereo matching deep convolutional neural networks, Ultramicroscopy 234 (2022) 113460.

[26] M. Weyland, P. A. Midgley, Electron tomography, Materials Today 7 (2004) 32-40.

[27] C. O. S. Sorzano, F. de Isidro-Gómez, E. Fernández-Giménez, D. Herreros, S. Marco, J. M. Carazo, C. Messaoudi, Improvements on marker-free images alignment for electron tomography, Journal of Structural Biology: X 4 (2020) 100037.

[28] E. Oveisi, A. Letouzey, D. T. L. Alexander, Q. Jeangros, R. Schäublin, G. Lucas, P. Fua, C. Hébert, Tilt-less 3-D electron imaging and reconstruction of complex curvilinear structures, Scientific Reports 7 (2017) 10630.

[29] J. Berthonneau, A. Obliger, P. L. Valdenaire, O. Grauby, D. Ferry,D. Chaudanson, P. Levitz, J. J. Kim, F. J. Ulm, R. J. M. Pellenq, Mesoscale structure, mechanics, and transport properties of source rocks' organic pore networks, Proceedings of the National Academy of Sciences 115 (2018) 12365–12370.

[30] J. Berthonneau, O. Grauby, I. C. Jolivet, F. Gelin, N. Chanut, Y. Magnin, R. J. M. Pellenq, D. Ferry, Nanoscale accessible porosity as a key parameter depicting the topological evolution of organic porous networks, Langmuir 37 (2021) 5464-5474.

[31] F. Appel, J. Paul, M. Oehring, Gamma titanium aluminide alloys (Wiley, 2011).

[32] G. Hug, A. Loiseau, and P. Veyssiere, Weak-beam observation of a dissociation transition in TiAl, Philosophical Magazine A 57 (1988) 499.

[33] J. P. Monchoux, A. Couret, L. Durand, T. Voisin, Z. Trzaska, M. Thomas, Elaboration of metallic materials by SPS: processing, microstructures, properties, and shaping. In: New trends in powder metallurgy (Multidisciplinary Digital Publishing Institute, 2021).

[34] T. Voisin, J. P. Monchoux, M. Perrut, A. Couret, Obtaining of a fine near-lamellar microstructure in TiAl alloys by Spark Plasma Sintering, Intermetallics 71 (2016) 88-97.

[35] H. Jabbar, J. P. Monchoux, F. Houdellier, M. Dollé, F. P. Schimansky, F. Pyczak, M. Thomas, A. Couret, Microstructure and mechanical properties of high niobium containing TiAl alloys elaborated by Spark Plasma Sintering, Intermetallics 18 (2010) 2312-2321.

[36] C. O. S. Sorzano, C. Messaoudi, M. Eibauer, J. R. Bilbao-Castro, R. Hegerl, S. Nickell, S. Marco, J. M. Carazo, Marker-free image registration of electron tomography tilt-series, BMC Bioinformatics 10 (2009) 124.

[37] C. Messaoudi, T. Boudier, C. O. S. Sorzano, S. Marco, TomoJ: tomography software for three-dimensional reconstruction in transmission electron microscopy, BMC Bioinformatics 8 (2007) 288.

[38] J. Darbon, A. Cunha, T. F. Chan, S. Osher, G. J. Jensen, 5th IEEE International Symposium on Biomedical Imaging: From Nano to Macro (Institute of Electrical and Electronics Engineers, 2008).

[39] A. Buades, B. Coll, J. M. Morel, Non-local means denoising, Image Processing On Line 1 (2011) 208-212.